

# Facile Measurement of Surface Heat Loss From Polymer Thin Films Via Fluorescence Thermometry

Gabriel Firestone <sup>1</sup>, Jason R. Bochinski,<sup>1</sup> Jeffrey S. Meth,<sup>2</sup> Laura I. Clarke<sup>1</sup>

<sup>1</sup>Department of Physics, North Carolina State University, Raleigh, North Carolina 27695-8202

<sup>2</sup>E. I. DuPont de Nemours & Co Inc, 200 Powder Mill Road, Wilmington, Delaware 19803

Correspondence to: L. I. Clarke (E-mail: laura\_clarke@ncsu.edu)

Received 14 September 2017; accepted 11 December 2017; published online 27 December 2017

DOI: 10.1002/polb.24571

**ABSTRACT:** Quantitative determination of heat loss and transport within complex systems having inhomogeneous temperatures and several different components is important for applications ranging from electronics to solar cells. An approach and material system to study heat transport within and heat loss from polymer thin films is presented. In a thin film configuration with a cylindrical heating source, the theoretical solution for temperature as a function of radial position can be determined from fundamental principles. Use of embedded fluorescent molecules as temperature probes and manipulation of the relative location of heating and thermometry light sources allows experimental measurements of

temperature versus position within the plane of the film. For a large range of practical cases, the exact theoretical solution can be well-approximated by a single term, which enables a fit to experimental data, and subsequent determination of either the heat loss coefficient at the film's surface or the material's effective thermal conductivity. © 2017 Wiley Periodicals, Inc. *J. Polym. Sci., Part B: Polym. Phys.* **2018**, *56*, 643–651

**KEYWORDS:** convective heat transfer; fluorescence thermometry; photothermal heating; polymer thin film; thermal properties

**INTRODUCTION** The heat transfer properties of homogeneous polymer systems are relatively well studied and understood. However in practice, materials are often formed into polymer composites, blends, or layered or interleaved systems.<sup>1</sup> Measuring the ability of such aggregate, complex materials to conduct or dissipate heat is important for applications varying from electronics to solar cells,<sup>2,3</sup> and may be especially useful for efficient testing during development of new material heat management systems. In this work, a straightforward technique is described by which the heat loss from a thin film surface can be ascertained via measurement of the radial (i.e., within the plane of the film) temperature distribution when spot heated with a laser. Temperature versus position is determined by fluorescence thermometry from molecules dispersed within the polymer. We discuss how this technique can also be utilized to determine heat transfer through the material.

Such an approach has several useful and flexible attributes. For thin films and coatings, the predominant heat loss occurs through the top and bottom surfaces, however direct measurement of the thermal gradients perpendicular to the thin film direction is experimentally challenging.<sup>4</sup> Here, the other

dimension is utilized by measuring the temperature distribution generated by a narrowly-confined circular heat source as a function of radial distance within the thin film plane. The mathematical connection between perpendicular and radial heat transport can then be utilized to quantitatively determine the heat loss from the thin film surfaces.

Fitting the radial temperature profile determines  $h = H/k$  where  $H$  is the convective heat transport coefficient characteristic of the heat loss at the surface and  $k$  is the thermal conductivity of the polymer system through which the heat travelled. When the thermal conductivity  $k$  is well known, as in the proof-of-principle work presented here employing a homogeneous, well-studied polymer, then  $H$  can be determined quantitatively. However, the surface heat loss coefficient is predominantly determined by the surrounding environment (i.e., the presence or absence of forced convection) and thus, in many cases, will be independent of material specifics and only depend on controllable external conditions. As a result, if the convective heat transport coefficient ( $H$ ) is known for a certain set of experimental conditions, then the effective thermal conductivity ( $k$ ) of the underlying material (including composites or layered structures) can in principle be readily determined.

Additional Supporting Information may be found in the online version of this article.

© 2017 Wiley Periodicals, Inc.

The ability to generate a heated region within the material and to measure the resultant radial temperature distribution is crucial to this approach. This strategy is synergistic with commercially-relevant heat management problems, where heat is generated in the interior of a structure and then must move outwards to be removed. In the present work, light is used to both create heat (via embedded metal nanoparticles) and measure the temperature (from fluorophores dispersed within the polymer). Specifically, a dilute concentration of gold nanoparticles is incorporated within the polymer film. When illuminated with light having a wavelength matching the particle's localized surface plasmon resonance<sup>5–7</sup> heat is generated within the material via a photo-thermal process.<sup>8–16</sup> This heating scheme is non-contact, highly efficient, and can easily be incorporated into a range of polymeric systems. As demonstrated below, photothermal heating provides an effective strategy to generate heat from within a material system. However, such spatially confined heating could alternatively be accomplished by doping with any moiety (e.g., carbon black or a non-fluorescent dye) which strongly absorbs the excitation light source. A different wavelength of light is utilized to excite the fluorescent molecule perylene, which is also randomly distributed throughout the polymer. As some of the co-authors have previously demonstrated,<sup>11,15,17,18</sup> a ratiometric measurement of the perylene fluorescence at different wavelengths can be used as a thermometer. Molecular thermometry and controlled positioning of the relative location of the heating and thermometry light sources (laser beams) provide sufficient spatial resolution (on the scale of 0.01 mm) to adequately sample the radial temperature profile. Although in the work discussed here the fluorescent molecules (perylene) utilized for spatially-resolved thermometry and the heating elements (gold nanoparticles) are both embedded within the polymer under study because heat transport depends on all elements in the system, in principle, such a test film could be layered between materials of unknown thermal properties (an approach which would require no special modification of the sample material under measurement).

The most common spatially-resolved non-contact temperature measurement techniques are thermochromic coatings,<sup>19,20</sup> infrared thermography,<sup>21–24</sup> and fluorescent molecular thermometry<sup>25,26</sup> (used in this work). Infrared thermography can measure a wide temperature range with minimal modification to the object under test. However, the complete optical path between object and detector must be known in order to ensure a reliable measurement, since many materials absorb infrared radiation. Spatial resolution of temperature along the beam path is not possible. Thermochromic coatings transmit temperature information in the visible range. However, thermochromic approaches only access relatively small temperature ranges and the associated materials degrade at elevated temperature. Fluorescent molecules, in this case perylene, retain the advantages of thermochromic coatings, while also possessing enhanced thermal and UV stability. There are many different approaches for fluorescent thermometry<sup>27–30</sup> including immobilization of sensors on a scanning probe tip.<sup>31</sup> Selective placement of

fluorophores within the material (our approach) enables temperature measurement from a specific portion of a complex sample (e.g., potentially, from a single layer within a multi-layered structure), and spatial resolution is limited only by the diffraction of the excitation source. Perylene is a commercially-available small molecule (minimizing perturbation to the polymer), stable to 300 °C (and thus suitable for extended use at elevated temperatures) with an emission structure with multiple features which can be used to establish an internal standard (a ratio independent of laser intensity, see subsequent sections).

In this work, fluorescence thermometry is utilized to determine the heat loss from a polymer thin film. The results are compared with existing estimates. The mathematical treatment which underlies these analyses is presented, and we discuss more general application of the technique to determine effective thermal conductivity of unknown materials.

## EXPERIMENTAL

### Sample Preparation

The Frens method was used to produce gold nanoparticles (AuNP).<sup>32</sup> Three hundred milliliters of an aqueous solution of tetrachloroauric(III) acid (Sigma-Aldrich) at 0.01 weight-percent (wt%) was brought to 95 °C. Once a stable temperature was achieved, 3 ml of 2 wt% sodium citrate (Sigma-Aldrich) was added to reduce the precursor and produce gold nanospheres. The mixture was maintained at 95 °C for 60 minutes as the color changed from clear to blue and finally red. After cooling, 0.002 wt% polyvinylpyrrolidone (PVP) (360 kg mol<sup>-1</sup>, Scientific Polymer Products, Inc.) was added to the solution to act as an additional stabilizing agent. Nanoparticles were characterized with transmission electron microscopy (TEM) (JEM 2000FX) and found to be roughly spherical (Supporting Information Figure S4) with an average diameter of 19 ± 7 nm (*N* = 75). The nanoparticles were transferred to dimethylformamide (DMF) (Sigma-Aldrich) via solvent exchange to enable dispersed incorporation within the poly(methyl methacrylate) (PMMA) (350,000 M<sub>w</sub>, Sigma-Aldrich) films. First, water was removed from the sample by heating to 60–65 °C for 5 days. Then DMF was added slowly over two days while maintaining the temperature at 60–65 °C to evaporate the remaining water.

Extinction spectroscopy (Cary 50 Scan) was utilized to further characterize the nanoparticles. The peak position of the localized surface plasmon resonance for the as-made gold nanoparticles in water, the suspension in DMF, and the particles in the final PMMA films (Fig. 5) were 521 nm, 532 nm, and 537 nm respectively, with FWHM (full width at half maximum) values of 104 nm, 130 nm, and 150 nm. The original peak location in water is consistent with the theoretical expectation of 524 nm for a ~18–19 nm diameter spherical gold nanoparticle. Slight spectral shifts in peak location which occur when comparing particles embedded in various material systems (e.g., solvent or polymer matrix) are expected due to differences in the dielectric constant of the surroundings. The concentration of the Au nanoparticle

dispersion in DMF was 29 nM as determined from the peak absorption at 532 nm utilizing an estimated extinction coefficient of  $7 \times 10^8$  ( $M^{-1} \text{ cm}^{-1}$ ),<sup>33</sup> with a residual water content less than 5%. This concentration matches well with the limiting maximum value (39 nM) if all gold atoms in the original solution formed 18.5 nm particles and then were incorporated into DMF with no losses. The stability of the peak width and lack of significant shifts in peak location indicate that the particles are well-dispersed in the final PMMA sample (see below for fabrication details).

Solutions of 0.1 wt% perylene in DMF and 10 wt% PMMA in DMF were prepared. One hundred and thirty microliters of the AuNP dispersion and 50  $\mu\text{l}$  of the perylene solution were added to 10 grams of the PMMA solution to produce a homogeneous coating solution. The formulation was drop-cast onto a glass coverslip that had been cleaned by ultraviolet-ozone treatment (Procleaner 110, Bioforce Nanoscience) for 30 minutes. The final PMMA films contained 0.02 wt% AuNP and 0.005 wt% perylene. Figure 5 shows AuNP and perylene extinction in the final films. The AuNP:PMMA concentration, determined from the height of the peak at 537 nm, was 5.8 nM consistent with the limiting value of 5.9 nM (from the known concentration of the AuNP in water). Similarly, the expected concentration of perylene was 230  $\mu\text{M}$  consistent with the observed value of 190  $\mu\text{M}$ . Samples were placed on a 65 °C hotplate for 12 hours to dry, after which films were removed by submerging in water. Typical film thickness was  $0.16 \pm 0.02$  mm as measured using digital calipers.

### Temperature Measurement and Data Analysis

As discussed in detail in previous works,<sup>11,15–18,34</sup> perylene molecules distributed throughout a polymeric material can act as a non-contact temperature sensor with high spatial resolution, limited by the probing laser beam diameter size and in this case, relative positioning of the heating and thermometry beams. Under a weak excitation source, perylene is stable under continuous illumination at elevated temperatures (up to 100 °C in PMMA in this work) for days with insignificant observed photobleaching. We expect that the technique described here should operate without loss of spatial resolution (see subsequent sections) for sample temperatures up to 200 °C, which is the useful temperature range (avoiding flow or degradation) for most polymer systems. Perylene was excited with a  $\sim 0.4$  mm diameter,  $\sim 5$   $\mu\text{W}$  power, 405 nm probing laser beam. The resulting fluorescence was spectrally-filtered through a scanning monochromator (Spex 1680b) onto a photomultiplier tube (Hamamatsu 931b), amplified, and photon counted (Stanford Research Systems SR400).

Figure 1(a) depicts an enhanced view of the pertinent portion of the detected perylene emission spectrum, showing the first two fluorescence peaks, which corresponds to emission from the lowest two vibrational levels of the first excited state. These spectra demonstrate that at elevated temperatures, each peak broadens, which means that the

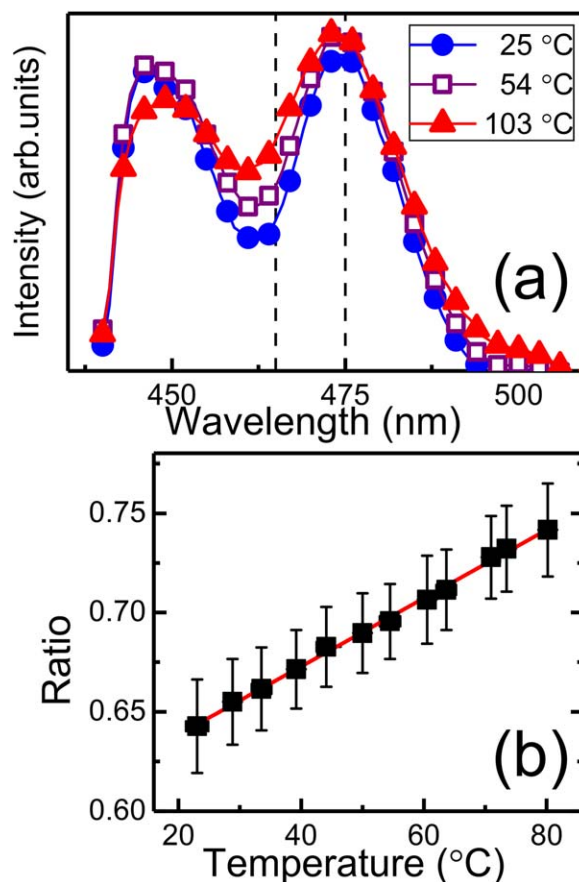


**FIGURE 1** (a) Measured fluorescence spectrum for perylene in the spectral range of interest at several temperatures. Vertical dashed lines indicate locations used to determine the ratio. (b) Intensity ratio of perylene fluorescence at varying sample temperatures under 405 nm excitation, with linear fit. [Color figure can be viewed at [wileyonlinelibrary.com](http://wileyonlinelibrary.com)]

peak amplitude relative to the “trough” region between peaks decreases. Figure 1(b) shows that the subsequent ratio of the first trough ( $\sim 465$  nm) to the second peak ( $\sim 475$  nm) varied linearly with the sample temperature when uniformly heated by a hotplate. These particular wavelength locations were selected by analyzing all possible ratio pairs to determine the combination that provided the most linear response to temperature over the range of interest.

To determine temperature versus position profiles, two ends of the free standing PMMA:AuNP:perylene films were supported by an aluminum bar with a free standing central portion (where the measurement takes place). Measurements could be performed on the free-standing films either under natural convection (no air flow control) or forced convection, where 16.4 CFH room temperature air was directed parallel to the film surface by a  $0.89'' \times 0.89''$  square aperture for a calculated average wind speed of  $25 \text{ cm s}^{-1}$ .

A 532 nm, 4 W continuous-wave diode laser was power-controlled with a rotating half-wave plate (Melles-Griot) followed by a fixed Glan-Laser polarizer (Thorlabs), and

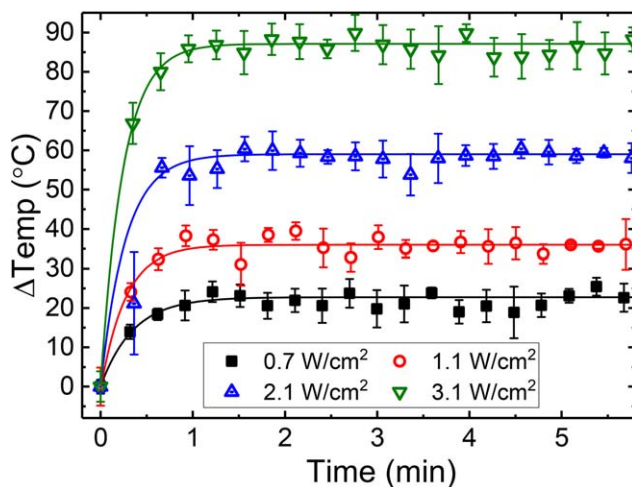


**FIGURE 2** Measured temperature increase in PMMA:AuNP:perylene film after a stationary heating beam is applied at time  $t=0$  for the stated intensities. Curve is a single exponential growth fit. All temperatures were within measured error of the steady state temperature 1 minute after laser application. [Color figure can be viewed at [wileyonlinelibrary.com](http://wileyonlinelibrary.com)]

position-controlled by a 2-axis mirror galvanometer system (SpaceLas PT-20k), ultimately passing through the sample from above, causing the embedded AuNP to heat the surrounding polymer matrix. A custom circuit was used to interface the galvanometric mirrors to a computer control system via a 12-bit digital-to-analog interface, leading to a nominal spatial resolution of  $\sim 5 \mu\text{m}$ . The control program could change mirror position with a time resolution of 300  $\mu\text{s}$ . In a typical experiment, however, the heating beam was moved very slowly and periodically to approximate steady state, traveling 16 mm across the film surface with a period of  $\sim 250$  minutes (or equivalent surface speed of 0.13 mm/minute). This slow scanning rate ensures that the system is in steady state, as needed for exact interpretation of the data. Figure 2 displays experimental measurements of temperature versus time during stationary excitation with the heating and probing beam overlapped (and neither moving). Equilibrium is established within 1 minute, independent of intensity over this range.

A portion near the center of the sample was illuminated from above with the 405 nm probing laser, exciting the embedded perylene molecules. The resulting temperature measured by the thermometry laser beam (which is stationary to enable efficient coupling to the subsequent analysis optics) was recorded as a function of the heating beam to thermometry beam distance. Figure 3 is the schematic of this approach, showing a cross-section of the film and two applied light beams. In practice, the heating beam's position was very slowly scanned (as described in the previous paragraph) over a line centered on the thermometry spot (i.e., to vary the heating-thermometry distance from c.a. - 8 mm to c.a. + 8 mm) in steps of 0.005 mm. Presented data (Figs. 4 and 8) is an average of 5–10 position sweeps. Data was manipulated in Origin and fit with a second order Bessel

function using the built-in Levenberg-Marquardt fitting algorithm for nonlinear fitting.

### Theoretical Background

Following the approach of Carslaw and Jaeger,<sup>35</sup> the polymer film is treated as a rectangular slab, extending infinitely in the  $x$ - and  $y$ - directions, and bounded in the  $z$ -direction by planes at  $z=0$  and  $z=l$ . The slab is initially at zero temperature and has convective boundary conditions at the surfaces into a medium at zero temperature. In practice, this assumption is that heat flux (energy per time per area) is linearly proportional to the difference between the local sample temperature and the temperature of the surroundings with  $H$  as the proportionality constant. Although these initial conditions are specific, the portion of the result utilized for fitting in the present work is independent of the particular boundary constraints. Let  $v$  be the temperature at any location  $(x, y, z)$  at time  $t$  due to an instantaneous point source of strength unity generated at  $(x', y', z')$  at time  $t=0$ . The solution is such that

$$\frac{\partial v}{\partial t} - \kappa \nabla^2 v = 0 \quad (0 < z < l), \quad (1)$$

$$-\frac{\partial v}{\partial z} + hv = 0 \quad \text{at } z=0, \quad (2)$$

$$\frac{\partial v}{\partial z} + hv = 0 \quad \text{at } z=l. \quad (3)$$

Equation 1 is the heat equation for conduction inside an isotropic solid with  $\kappa$  the thermal diffusivity. Equations 2 and 3

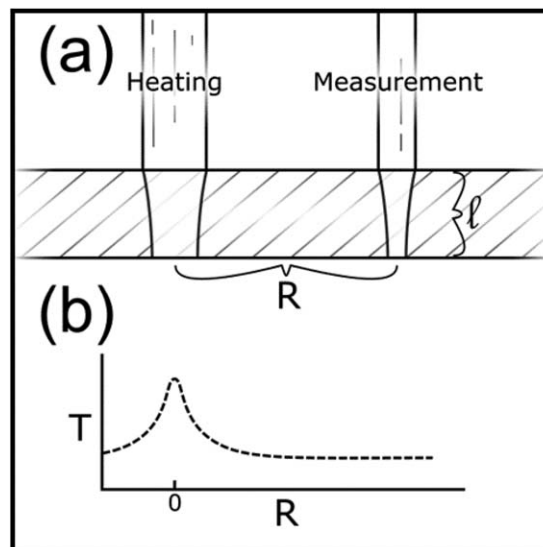


**FIGURE 3** (a) Schematic of the profile measurement, where a 532 nm heating laser beam incident from above excites gold nanoparticles embedded in a film of thickness  $l$ , while a 405 nm probing laser beam excites dispersed perylene to measure the film temperature. (b) When combined with the known separation  $R$  between the two laser beam spots, a temperature profile is created.

describe top and bottom surfaces such that the heat flux out of the slab is proportional to the surface temperature, where dividing the entire equation by  $k$  converts from energy to temperature. The goal of this work is to obtain a numerical value for the proportionality term  $h$ , which relates directly to the convective heat transfer coefficient  $H$  and thermal conductivity  $k$  by

$$h = \frac{H}{k}$$

For an instantaneous unit point source located at  $(x', y', z')$  the Green's function solution to the time dependent heat equation is

$$v(R, z, t, \kappa, h, l) = \frac{e^{-R^2/4\kappa t}}{2\pi\kappa t} \sum_{n=1}^{\infty} \frac{(\alpha_n \cos\alpha_n z + h \sin\alpha_n z)}{l(\alpha_n^2 + h^2) + 2h} * (\alpha_n \cos\alpha_n z' + h \sin\alpha_n z') * e^{-\kappa\alpha_n^2 t} \quad (4)$$

where  $R = \sqrt{(x-x')^2 + (y-y')^2}$  (the radial distance from the heat source) and  $\alpha_n$  are the positive roots of

$$\tan(\alpha l) = \frac{2\alpha h}{\alpha^2 - h^2} \quad (5)$$

The  $\alpha$  values connect the  $z$  and  $R$  portions of the solution, appearing in both. In order to establish a steady state result, the Laplace transform of the Green's function solution from the time domain  $t$  to the frequency domain  $s$  is

$$\bar{v}(p) = \frac{1}{\pi\kappa} \sum_{n=1}^{\infty} K_0 \left( \sqrt{\frac{(p + \kappa\alpha_n^2)R^2}{\kappa}} \right) \frac{(\alpha_n \cos\alpha_n z + h \sin\alpha_n z)}{l(\alpha_n^2 + h^2) + 2h} * (\alpha_n \cos\alpha_n z' + h \sin\alpha_n z'), \quad (6)$$

where  $p = \sqrt{s/\kappa}$  has been substituted for readability and  $K_0$  is the modified Bessel function of the second kind of order zero. For this simple case, the steady state temperature distribution because of a continuous source of strength  $Q$  (in watts) is found from the time-dependent solution for an instantaneous source by taking advantage of the theory of sources and sinks of heat through:

$$\lim_{t \rightarrow \infty} v(t) = \frac{\kappa Q \bar{v}}{k} \Big|_{p=0}, \quad (7)$$

resulting in a steady state expression of

$$\lim_{t \rightarrow \infty} v(R, z, t, \kappa, h, l) = \frac{Q}{\pi k} \sum_{n=1}^{\infty} K_0(\alpha_n R) \frac{(\alpha_n \cos\alpha_n z + h \sin\alpha_n z)}{l(\alpha_n^2 + h^2) + 2h} * (\alpha_n \cos\alpha_n z' + h \sin\alpha_n z'). \quad (8)$$

Thus in this work, a spot heating source is applied, the system comes to steady state, and the resulting spatial distribution of temperature is obtained, which can be modeled by eq 8. Notice that the radial dependence of this solution is solely contained within the  $K_0$  term, which is independent of  $z$ . As discussed in more detail in the next section, if there is a single dominant term in the sum, resulting in a truncation to one term, then the  $z$  solution acts as a constant with respect

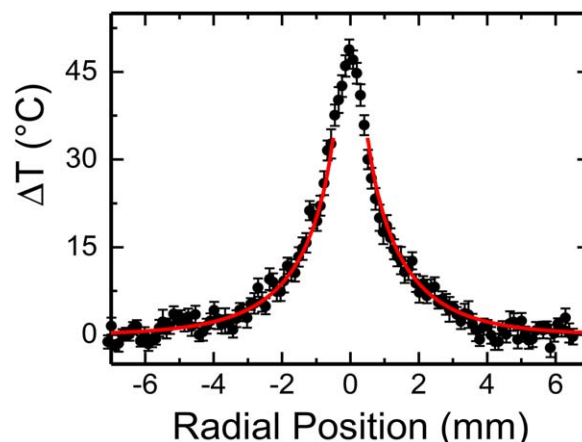


**FIGURE 4** Measured radial temperature (above ambient) profile of a 0.34 mm thick PMMA: AuNP: perylene film illuminated with a 1.9 mm diameter 532 nm heating laser beam. The red line is a fit in the spatial region  $|R| > 0.5$  mm. [Color figure can be viewed at [wileyonlinelibrary.com](http://wileyonlinelibrary.com)]

to  $R$ , and experimental measurements of the radial temperature distribution enable facile determination of the pertinent  $\alpha$ . Inserting this experimentally derived  $\alpha$  term along with the measured sample thickness  $l$  into eq 5 yields a value for  $h$ .

## RESULTS AND DISCUSSION

### General Approach and Limits

Figure 4 shows an experimental temperature profile for a 0.34 mm thick, free standing, thin film of PMMA doped with 0.02 wt% of gold nanoparticles and  $\sim 234 \mu\text{M}$  (0.005 wt%) of perylene, illuminated by a 1.90 mm  $\frac{1}{e^2}$  diameter,  $\sim 4.5 \text{ cm}^{-2}$  intensity 532 nm laser beam.

This excitation light overlaps with the localized surface plasmon resonance of the gold nanoparticles<sup>5-7</sup> (Fig. 5, thick vertical dashed line) and thus is strongly absorbed in a photothermal process, resulting in heating of the particles and subsequent delivery of thermal energy to the surrounding polymer.<sup>8-16,34,36,37</sup> These point-like heat sources are distributed homogeneously throughout the film sample (i.e., at  $z'$  varying from 0 to  $l$ ) and their heat flux output will depend on the intensity of the excitation light at their location. Perylene molecules uniformly dispersed throughout the sample serve as temperature sensors. A position-specific temperature is determined by applying a  $\sim 0.4$  mm diameter, low intensity ( $\sim 4 \text{ mW cm}^{-2}$ ) probing beam of 405 nm light which is selectively absorbed by the perylene (Fig. 4, thin vertical dotted line), resulting in fluorescence at wavelengths in the 430 to 575 nm range.

As previously demonstrated,<sup>11,15,17,18</sup> the emission features from the distinctive vibrational levels of perylene broaden and the peak amplitude reduces as the sample temperature increases. The ratio of the intensity near a peak location to that of the minimum between adjacent peaks is a quasi-linear function of temperature which can be utilized for

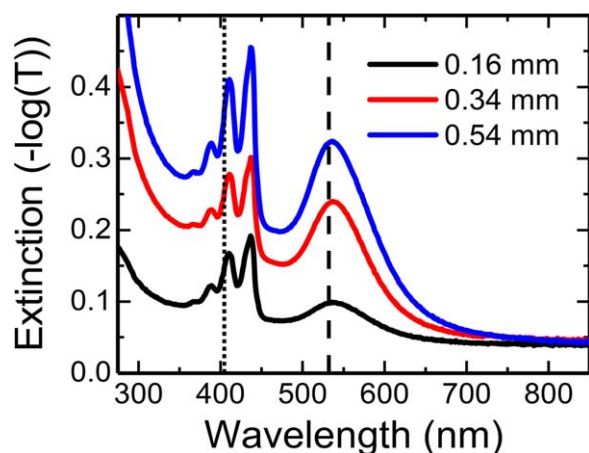


**FIGURE 5** Extinction spectra of PMMA nanocomposite films of varying thickness (0.16, 0.34, and 0.54 mm), containing gold nanoparticles and perylene. The vertical thick dashed (thin dotted) line indicates the spectral location of the 532 nm (405 nm) heating (thermometry) laser. The feature(s) centered  $\sim 535$  nm (between 375 and 435 nm) indicates the presence of AuNPs (perylene molecules). See Experimental section for further discussion. [Color figure can be viewed at [wileyonlinelibrary.com](http://wileyonlinelibrary.com)]

thermometry (see Experimental section). The data shown in Figure 4 are achieved by controllably manipulating the distance between the heating and thermometry beams: in effect, moving the thermometry beam relative to the heating beam to determine the temperature at each radial distance, which can be achieved to high spatial resolution via computer control of galvanometric mirrors that regulate the position of the heating beam.

Fitting the data with eq 8 enables deduction of the heat loss from the surface. The solution presented in eq 8 is an infinite sum (in  $n$ ) where each  $K_0$  term has a different radial dependence (because of the scaling of  $R$  by  $\alpha_n$ ). The  $\alpha_n$  values are solutions to eq 5. Analysis of this expression reveals that the first root  $\alpha_1$  has the greatest sensitivity to variation in  $h$ , the loss term, while increasing terms tend toward  $\alpha_n = \frac{n\pi}{l}$ . Because  $\alpha_n$  monotonically increases with  $n$ , higher order terms ( $K_0(\alpha_n R)$ ) decay more rapidly with  $R$  and thus primarily contribute at small  $R$  values. To gauge the contribution of larger  $n$  value terms to the final solution for the parameter space, we expect to explore, one can substitute reasonable numbers for  $H$ ,  $K$ , and  $l$  ( $10 \text{ W m}^{-2} \text{ K}^{-1}$ ,  $0.2 \text{ W m}^{-1} \text{ K}^{-1}$ , and  $1 \text{ mm}$  respectively) into the transcendental equation (eq 5) and compare the sum in eq 8 term-by-term for the resulting  $\alpha_n$ . This analysis is presented as Figure 6 and reveals that, for a reasonable range of expected values, the  $n=1$  term (solid black line) dominates for  $R$  values greater than  $0.5 \text{ mm}$ .

Considering the  $z$ -dependence of the solution, because molecular thermometry is utilized to determine temperature versus  $R$  profiles, depending on the specific experimental conditions (e.g., the depth of penetration of the light that excites the fluorophores), temperature information will

either be averaged over some range in the  $z$ -direction (up to  $z=[0, l]$  the entirety of the film) or predominantly reflect  $z=l$  (the upper surface). In either case, however, the  $z$ -dependent portion of the eq 8 is a constant for each  $n$  value. Thus, if the sum is truncated to  $n=1$ , then the solution reduces to a single radially-dependent term multiplied by an (a priori unknown) constant. Furthermore, study of a range of cases where the boundary conditions at  $z=0$  and  $z=l$  differ, reveals that these specifics only alter the form of the  $z$  component of the solution, leaving the form  $K_0(\alpha_1 R)$  of the  $R$  solution unchanged. Such an outcome means that  $h$  can be obtained by simply fitting with  $K_0(\alpha_1 R)$  in the  $R > 0.5 \text{ mm}$  range. In Figure 4, a typical temperature profile is fit (solid red line) by this truncated sum ( $n=1$  only) in the region  $|R| > 0.5 \text{ mm}$  and excellent agreement between the model and the measured profile is observed.

This solution [eq 8 or truncated versions] assumes that the heating source is point-like or equivalently, that the fit is applied outside the region where the azimuthally-symmetrical heating beam is present. To evaluate the contribution of the presence of non-negligible heating sources, the experimental temperature versus position curve (Fig. 4) was fit with  $K_0(\alpha_1 R)$  using various cutoff radii; that is, beginning the fit at  $R = R_{\text{cutoff}}$ , where  $R_{\text{cutoff}}$  ranged from  $0$  to  $2.0 \text{ mm}$ . The  $H$  values determined from these fits are summarized in Supporting Information Figure S1, and reveal three distinct regions. For  $R_{\text{cutoff}}$  values from  $0$  to  $0.5 \text{ mm}$  which overtly results in application of the solution to regions where a strong heating source is present,  $h$  is suppressed and increases rapidly in value with increasing  $R_{\text{cutoff}}$ , indicating the importance of the higher terms and the beam profile. If a strong heating source is present, temperature should fall less rapidly than expected, flattening the curve at low  $R$  and thus resulting in an artificially low  $\alpha$  and thus  $H$  values. In contrast, for  $R_{\text{cutoff}}$  from  $0.5$  to  $1.2 \text{ mm}$ , a stable region is observed, where  $H$  is independent of  $R_{\text{cutoff}}$ , as expected if the  $n=1$  term dominates and

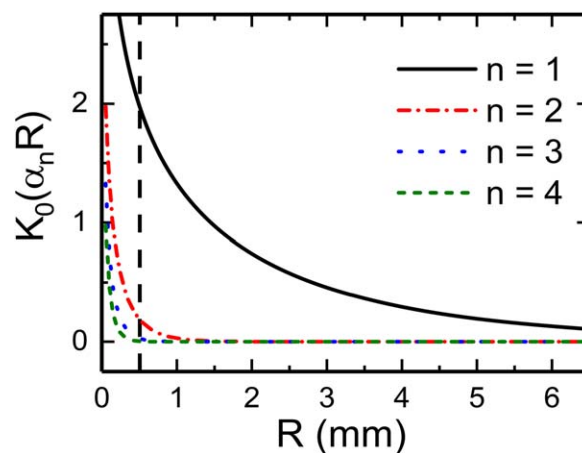


**FIGURE 6** Visualization of the relative contribution of successive  $n$  terms [eq. (8)] on the temperature distribution for reasonable values of  $H$ ,  $k$ , and  $l$ . The dashed vertical line indicates the  $R > 0.5 \text{ mm}$  cutoff region. [Color figure can be viewed at [wileyonlinelibrary.com](http://wileyonlinelibrary.com)]

the presence of the beam has only a minor effect. The  $\frac{1}{\sigma_z}$  radius of the heating beam utilized in this case is 0.95 mm. For  $R_{\text{cutoff}} > 1.2$  mm, where a larger fraction of data is approaching the background temperature and thus prone to noise and potentially difficult to fit,  $H$  and the error grow without limit.

Thus, from the minimum  $R_{\text{cutoff}}=0.5$  mm set by the truncation of the sum, the value of  $H$  obtained from the fit remained constant both inside and outside the  $\frac{1}{\sigma_z}$  radius of the heating beam until noise effects and excessive truncation of the raw data resulted in very large error values. This result held for all data sets (independent of sample thickness or irradiation intensity). In practice, the existence of such a stable range is reassuring that the fit is robust and that the correct value of  $H$  has been obtained. To include the most data possible and minimize error in the fit,  $R_{\text{cutoff}}=0.5$  mm was utilized for the remainder of this work.

### Surface Heat Loss Results

As an example of the conversion of  $\alpha$  to  $h$ , the fit shown in Figure 4 results in  $\alpha_1=530 \pm 20 \text{ m}^{-1}$ . Accounting for the measured sample thickness ( $l=0.34 \text{ mm}$ ) and the thermal conductivity of bulk PMMA ( $k=0.19 \text{ W m}^{-1} \text{ K}^{-1}$ ) and utilizing the transcendental equation 5, results in  $H=9.1 \pm 0.71 \text{ W m}^{-2} \text{ K}^{-1}$ . These values fall within the parameter space where eq 8 can be truncated by eliminating higher  $\alpha_n$ , which we confirmed by re-creating Figure 6 (see Supporting Information Figure S2). This value for  $H$  can be compared to available theoretical estimates for a horizontal plate under natural convection.<sup>38</sup> Utilizing a characteristic length equal to the heating laser beam  $\frac{1}{\sigma_z}$  diameter (1.9 mm) and assuming uniform heating to the observed peak temperature (50 °C), the predicted coefficients for the top and bottom surfaces,  $H_{\text{top}}=17 \text{ W m}^{-2} \text{ K}^{-1}$  and  $H_{\text{bot}}=8.6 \text{ W m}^{-2} \text{ K}^{-1}$ , are consistent with the value obtained from our approach. Note that while the uniform temperature assumption required for these theoretical estimates is incorrect (which may be related to the overestimate of the value for  $H_{\text{top}}$ ), more importantly, the experimental approach described here gives an accurate value for this specific circumstance (with innate heterogeneity) through a relatively simple measurement.

To verify the robustness of the method, the convective heat transfer coefficient was experimentally measured for different peak temperatures (using multiple heating laser intensities, Fig. 7, solid symbols) with films of varying thicknesses.  $H$  should be relatively independent of both these parameters, which is reflected by the data, resulting in an average value of  $H=10 \pm 1.9 \text{ W m}^{-2} \text{ K}^{-1}$  over the range of 20 °C–89 °C above room temperature (for film thicknesses of 0.16 to 0.54-mm). Measured  $H$  values gradually increase with peak temperature, in general agreement with  $H \propto T^{1/4}$  as predicted by theory for a uniformly heated horizontal plate (Supporting Information Figure S3).<sup>38</sup>

The radial temperature profile was also measured under forced convection of air (Fig. 7, open symbols) parallel to the film surface at  $25 \text{ cm s}^{-1}$  for the three different samples

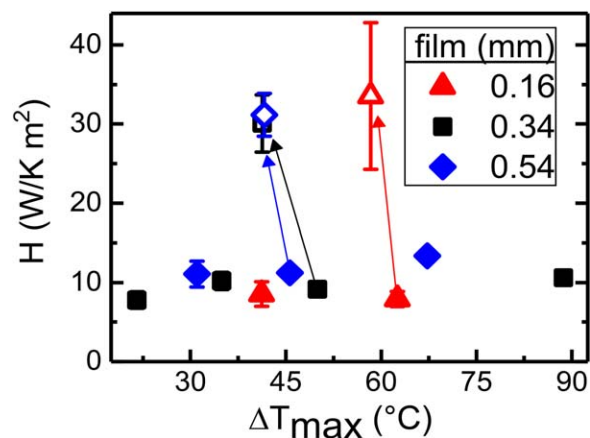


**FIGURE 7** Calculated convective heat transfer coefficient ( $H$ ) versus maximum sample temperature above ambient ( $\Delta T$ ) for several sample film thicknesses under different laser intensities with natural (solid data points) or forced (25 cm/s, open data points) convection. [Color figure can be viewed at wileyonlinelibrary.com]

thicknesses at 3.2, 4.6, and 6.7  $\text{W cm}^{-2}$  excitation light intensities, resulting in a final temperature range of 40 - 60 °C. As shown in Figure 7 (open symbols), the increased heat transfer results in a reduced peak temperature (compared to the corresponding case at the same thickness and heating laser intensity without forced convection) and an elevated  $H$  value. The effect of forced convection is also seen clearly (Fig. 8) as a narrowing of the temperature profile, indicating that heat is lost through the top and bottom surfaces before it conducts radially towards unheated regions of the sample. The measured  $H=30 \pm 3.6 \text{ W m}^{-2} \text{ K}^{-1}$  can be compared to the expected value for a horizontal plate with an unheated leading edge under laminar forced convection with a characteristic length equal to the unheated edge length plus the heating

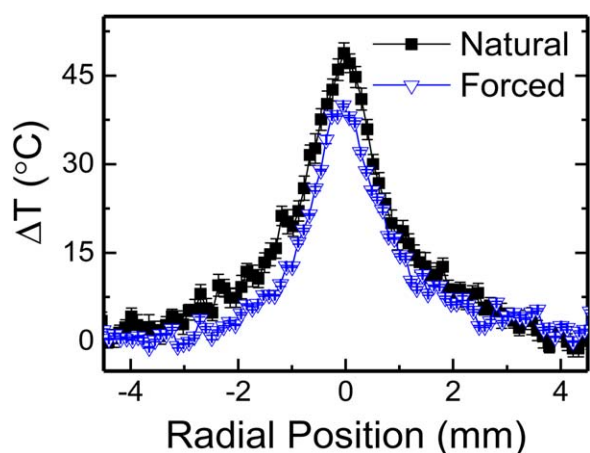


**FIGURE 8** Comparison of radial temperature profiles above ambient of a 0.34 mm thick AuNP-PMMA nanocomposite film illuminated with 1.9 mm diameter, 65 mW, 532 nm heating laser beam under natural (solid black squares) and forced (25 cm/s airflow across the surface, open blue triangles) convection. [Color figure can be viewed at wileyonlinelibrary.com]

laser spot diameter. The predicted value of  $H=27$   $\text{W m}^{-2} \text{K}^{-1}$  is in agreement with the experimentally measured value.<sup>39</sup>

Overall these results indicate that measurement and analysis of the temperature profile resulting from cylindrical heating of a region of a polymer film, can be utilized to determine  $H$  if  $k$  is known. Conversely, because  $h$  is simply a ratio, measuring a similar-thickness film of unknown  $k$  under the same experimental conditions should yield an  $H$  value of approximately  $10 \text{ W m}^{-2} \text{K}^{-1}$  under natural convection and approximately  $30 \text{ W m}^{-2} \text{K}^{-1}$  when exposed to the  $25 \text{ cm s}^{-1}$  air flow parallel to the film surface. Thus, the following procedure could be utilized: For a particular experimental arrangement, samples of well-known materials are measured to determine the expected  $H$  for a thin film due to convective and conductive losses to the surrounding air. Then the same experiments are repeated with an unknown material, which could be a layered structure including the heating/measurement films,  $h$  is determined and then an effective  $k$  is calculated from the known  $H$  value.

## CONCLUSIONS

In a thin film configuration, the theoretical solution for temperature as a function of position due to local heating from a small diameter laser beam can be determined from fundamental principles. The result has several properties that make it useful for determining either the thermal conductivity  $k$ , or  $H$ , where  $H*(T-T_{\text{ambient}})$  is the energy lost per time per area from the film's surfaces. The solution is a product of functions that depend exclusively on either  $z$  or  $R$ . This enables measurement of the radial temperature profile, which is generally experimentally accessible, to serve as a tool for subsequent determination of the perpendicular heat loss from top and bottom surfaces. Although the solution is a sum of modified Bessel functions (plus possible convolution with the beam profile of the heating source), under many pertinent experimental conditions, utilizing the leading term to fit temperature versus distance outside of the most strongly irradiated area is a highly accurate approximation. Under those conditions, the specifics of the  $z$ -dependence are unimportant, and the perpendicular heat loss can be determined irrespective of the position of the heating and temperature measurement layers and the specific boundary conditions.

This theoretical analysis is particularly useful when paired with fluorescence thermometry whereby temperature versus radial position can be easily measured with relatively high spatial resolution. In particular, a heating beam (that will excite photothermal heating via overlap with the surface plasmon resonance of embedded gold nanoparticles) and a thermometry beam (which measures temperature via perylene fluorescence) are manipulated with galvanometric mirrors to controllably and precisely alter their relative positions and trace out temperature versus position with the plane of the film. By making such measurements for samples with a known thermal conductivity the effective heat loss

coefficient (e.g., the convective heat transfer coefficient if convection is the dominant heat loss mechanism) can be determined. Alternatively, if the effective heat loss coefficient under particular experimental conditions is well-known, the thermal conductivity of a novel sample can be determined. This type of theoretical analysis could be paired with any source of temperature profile data, such as IR thermography, where two-dimensional profile data could be used for studying anisotropy<sup>21</sup> or rotational signal averaging could be used to form the temperature profile.

## ACKNOWLEDGMENTS

This research was supported by the National Science Foundation (grants CMMI-0829379, CMMI-106910). Additionally, the authors thank Prof. Keith Weninger (NCSSU) for use of equipment and Prof. Russell Gorga for useful discussions. This work was performed in part at the Analytical Instrumentation Facility (AIF), which is supported by the State of North Carolina and the National Science Foundation (grant ECCS-1542015). The AIF is a member of the North Carolina Research Triangle Nanotechnology Network (RTNN), a site in the National Nanotechnology Coordinated Infrastructure (NNCI).

## REFERENCES AND NOTES

- 1 I. A. Tsekmes, R. Kochetov, P. H. F. Morshuis, J. J. Smit, In *Proc. IEEE International Conference on Solid Dielectrics IEEE*, Bologna, Italy **2013**; 678.
- 2 S. V. Garimella, A. S. Fleischer, J. Y. Murthy, A. Keshavarzi, R. Prasher, C. Patel, S. H. Bhavnani, R. Venkatasubramanian, R. Mahajan, Y. Joshi, B. Sammakia, B. A. Myers, L. Chorosinski, M. Baelmans, P. Sathyamurthy, P. E. Raad, *IEEE Trans. Compon. Packag. Technol.* **2008**, *31*, 801.
- 3 A. I. Kudish, E. G. Evseev, G. Walter, T. Leukefeld, *Energy Convers. Manag.* **2002**, *43*, 651.
- 4 P. R. N. Childs, J. R. Greenwood, C. A. Long, *Proc. Instn. Mech. Eng.* **1999**, *213*, 655.
- 5 L. M. Liz-Marzan, *Langmuir* **2006**, *22*, 32.
- 6 S. Eustis, M. A. El-Sayed, *Chem. Soc. Rev.* **2006**, *35*, 209.
- 7 S. Link, M. A. El-Sayed, *J. Phys. Chem. B.* **1999**, *103*, 8410.
- 8 Z. Qin, J. C. Bischof, *Chem. Soc. Rev.* **2012**, *41*, 1191.
- 9 T. Ding, V. K. Valev, A. R. Salmon, C. J. Forman, S. K. Smoukov, O. A. Scherman, D. Frenkel, J. J. Baumberg, *Proc. Natl. Acad. Sci.* **2016**, *113*, 5503.
- 10 P. K. Jain, X. Huang, I. H. El-Sayed, M. A. El-Sayed, *Acc. Chem. Res.* **2008**, *41*, 1578.
- 11 S. Maity, J. R. Bochinski, L. I. Clarke, *Adv. Funct. Mater.* **2012**, *22*, 5259.
- 12 S. Lal, S. E. Clare, N. Halas, *J. Acc. Chem. Res.* **2008**, *41*, 1842.
- 13 A. O. Govorov, H. H. Richardson, *Nano Today*. **2007**, *2*, 30.
- 14 S. Maity, L. N. Downen, J. R. Bochinski, L. I. Clarke, *Polymer* **2011**, *52*, 1674.
- 15 S. Maity, W. C. Wu, C. Xu, J. B. Tracy, K. Gundogdu, J. R. Bochinski, L. I. Clarke, *Nanoscale* **2014**, *6*, 15236.
- 16 S. Maity, K. A. Kozek, W. C. Wu, J. B. Tracy, J. R. Bochinski, L. I. Clarke, *Part. Part. Syst. Charact.* **2013**, *30*, 193.

- 17** D. B. Abbott, S. Maity, M. T. Burkey, R. E. Gorga, J. R. Bochinski, L. I. Clarke, *Macromol. Chem. Phys.* **2014**, *215*, 2345.
- 18** V. Viswanath, S. Maity, J. R. Bochinski, L. I. Clarke, R. E. Gorga, *Macromolecules* **2013**, *46*, 8596.
- 19** V. U. Kakade, G. D. Lock, M. Wilson, J. M. Owen, J. E. Mayhew, *Int. J. Heat Fluid Flow*. **2009**, *30*, 939.
- 20** S. V. Ekkad, J. C. Han, *Meas. Sci. Technol.* **2000**, *11*, 957.
- 21** D. N. Simavilla, D. C. Venerus, *J. Heat Transf.* **2014**, *136*, 111303.
- 22** A. Salazar, A. Mendioroz, R. Fuente, *Appl. Phys. Lett.* **2009**, *95*, 121905.
- 23** G. M. Carlomagno, G. Cardone, *Exp Fluids*. **2010**, *49*, 1187.
- 24** H. Robotjazi, H. Zhao, D. F. Swearer, N. J. Hogan, L. Zhou, A. Alabastri, M. J. McClain, P. Nordlander, N. J. N. Halas, *Nat. Commun.* **2017**, *8*, 27.
- 25** A. Assy, H.-J. Lin, M. Schoenauer-Sebag, P. Gredin, M. Mortier, L. Billot, Z. Chen, L. Aigouy, *Sensors Actuators A Phys.* **2016**, *250*, 71.
- 26** L. M. Maestro, P. Haro-González, J. G. Coello, D. Jaque, *Appl. Phys. Lett.* **2012**, *100*, 201110.
- 27** E. Saïdi, J. Labéguerie-Egée, L. Billot, J. Lesueur, M. Mortier, L. Aigouy, *Int. J. Thermophys.* **2013**, *34*, 1405.
- 28** C. W. Meyer, D. C. Meier, C. B. Montgomery, S. Semancik, *Sensors Actuators A Phys.* **2006**, *127*, 235.
- 29** P. Löw, B. Kim, N. Takama, C. Bergaud, *Small* **2008**, *4*, 908.
- 30** M. Kim, M. Yoda, *J. Heat Transfer*. **2011**, *134*, 11601.
- 31** L. Aigouy, G. Tessier, M. Mortier, B. Charlot, *Appl. Phys. Lett.* **2005**, *87*, 184105.
- 32** G. Frens, *Nat. Phys. Sci.* **1973**, *241*, 20.
- 33** W. Haiss, N. T. K. Thanh, J. Aveyard, D. G. Fernig, *Anal. Chem.* **2007**, *79*, 4215.
- 34** J. Dong, G. E. Firestone, J. R. Bochinski, L. I. Clarke, R. E. Gorga, *Nanotechnology* **2017**, *28*, 065601.
- 35** Carslaw, H. S., Jaeger, J. C., *Conduction of Heat in Solids*, 2nd ed.; Oxford Clarendon Press, Oxford, Great Britain, **1959**, 373.
- 36** V. Viswanath, S. Maity, J. R. Bochinski, L. I. Clarke, R. E. Gorga, *Macromolecules*. **2016**, *49*, 9484.
- 37** S. Maity, W.-C. Wu, J. Tracy, L. Clarke, J. Bochinski, *Nanoscale*. **2017**, *9*, 11605.
- 38** W. H. McAdams, *Heat Transmission*, 3rd ed.; McGraw-Hill, New York, NY, **1958**.
- 39** W. M. Kays, M. E. Crawford, *Convective Heat and Mass Transfer* 3rd ed.; McGraw-Hill, New York, NY, **1980**.